Metrol. Meas. Syst., Vol. 30 (2023) No. 3, pp. 507–518
DOI: 10.24425/mms.2023.146418

PAN POLSKA AKADEMIA NAUK

METROLOGY AND MEASUREMENT SYSTEMS
Index 330930, ISSN 0860-8229
www.metrology.wat.edu.pl

M&MS

IDENTIFICATION OF CLADDING MODES IN SMF-28 FIBERS WITH TFBG STRUCTURES

Piotr Kisała[1)], Aliya Kalizhanova[2,3)], Ainur Kozbakova[2)], Bakhyt Yeraliyeva[4)]

1) Lublin University of Technology, Nadbystrzycka 38A, 20-618 Lublin, Poland (✉ *p.kisala@pollub.pl*)
2) Institute of Information and Computational Technologies CS MES RK, 050010, 125 Pushkin str., Almaty, Republic of Kazakhstan (*ainur79@mail.ru*)
3) Almaty University of Power Engineering and Telecommunications named after Gumarbek Daukeyev, Almaty 050010, Kazakhstan, Almaty, Shevshenko 28 (*kalizhanova_aliya@mail.ru*)
4) Taraz State University after M.Kh. Dulaty, Tole Bi St 40, Taraz, Republic of Kazachstan (*b_eral@mail.ru*)

Abstract

This article proposes an unequivocal method of labeling and numbering the cladding modes propagating in single-mode optical waveguides with tilted periodic structures. The unambiguous determination of individual propagating modes in this type of optical fiber is crucial for their use in sensory systems. The selection of the appropriate spectral range and mode determines the sensitivity and measuring range of tilted fiber Bragg grating (TFBG) sensors. The measurement methods proposed by individual research teams using TFBGs as transducers are usually based on the selection of specific modes. Unification of the labeling of modes and their numbering enables comparison of the basic metrological parameters of individual measurement methods and reproduction and verification of the proposed sensors and methods in the laboratories of other scientific and research centers.

Keywords: optical fiber sensors, tilted fiber Bragg gratings, optical measurements.

1. Introduction

The use of phenomena occurring during the propagation of an electromagnetic wave, particularly its diffraction or scattering [1], allows the measurement of many other phenomena and physical quantities, even the size of particles [2,3]. Periodic disturbances of an optical medium in the form of optical diffraction Bragg gratings are used as sensors that are modern, fast [4], insensitive to electromagnetic interference [5], and small sized [6]. Consequently, they can be used in *e.g.*, explosive hazardous environments to detect many physical quantities and physical decomposition [7]. Their 3D modifications in the form of *tilted fiber Bragg grating* (TFBG) structures significantly expand the spectrum of their applications [8] and open up a range of possibilities for new measurements, *e.g.*, measurement of the concentration of various substances in aqueous solutions [9], refractometry [10], measurement of the light polarization plane [11,12] and many others.

Article history: received March 9, 2023; revised May 7, 2023; accepted May 14, 2023; available online September 15, 2023.

The analysis of the transmission properties of TFBG structures subjected to bending [13], stretching [14], immersion in liquids [15] and solutions [16], temperature changes [15], rotation [17], torsion [18] and many other factors is significantly facilitated if the numbering of individual cladding modes propagating through such structures is introduced. Optical fibers often have a step discontinuity in the refractive index at the core-cladding interface. Such fibers can be treated as cylindrically symmetrical dielectric waveguides which can be used to model the propagation of the introduced electromagnetic wave. Modes that can propagate in such fibers are divided into several groups based on the electric and magnetic field strengths in relation to the direction of propagation of the electromagnetic wave in the waveguide. The first group includes modes whose electric field strength in the direction of propagation of the electromagnetic wave is zero. They are labeled TE modes (electric field transverse to the propagation direction). The second group includes modes whose magnetic field strength in the direction of propagation of the electromagnetic wave is zero. These in turn are labeled TM modes (magnetic field transverse to the propagation direction). The third group consists of hybrid modes labeled HE and EH in which both the electric field strength and magnetic induction along the direction of propagation of the electromagnetic wave are zero. For typical fibers used in telecommunications and data transmission systems, the difference in the refractive index between the core and the cladding is so small (*e.g.*, 0.001-0.01) that most TE, TM and hybrid modes are degenerate, and use of only one designation for all these modes is sufficient. The most common designation is then LP modes (*linearly polarized modes*) [19]. Each LP mode is defined as LP_{mn}, where the indices m and n are related to the number of radial and azimuthal zeros of the particular mode.

The basic mode is LP_{01}. It is the only mode that can propagate in a single-mode fiber. Nevertheless, the appearance of a periodic structure in the waveguide whose planes are at a certain angle (θ) in relation to the direction of propagation of the electromagnetic wave causes part of the energy of the LP_{01} mode to be coupled to higher order modes, which propagate in the cladding over a certain distance where they are strongly suppressed. Since in a single-mode fiber, these modes quickly decay and only the LP_{01} mode remains, which propagates in the core of the waveguide, adjacent minima are visible in the transmission spectrum for wavelengths corresponding to higher-order modes. In the case of TFBG structures written in single-mode fibers, only the LP_{0n} and LP_{1n} modes are excited among the whole range of LP_{mn} modes [20]. Linearly polarized modes LP_{0n} are also called zero-order modes or modes with azimuthal number 0, while modes LP_{1n} are called second-order modes or modes with azimuthal number 1 [21, 22]. This nomenclature will also be used in a subsequent part of this study. Linearly polarized modes are treated as a set of minima forming a comb in the transmission spectral characteristics. In specific applications of TFBG structures, *e.g.*, sensor structures, an extremely important but also interesting issue is the difference in the measured response values of individual modes. This article addresses a method for unambiguous numbering of the modes in TFBG structures, which can be used to measure bending, the polarization angle of input light and many other physical quantities.

The spectral characteristics of the TFBG structure produced in the core of a single-mode fiber are shown in Fig. 1. The grating has a diffraction plane tilt angle equal to 2°, and the input light is polarized according to the P state [11]. The entire structure has a length of 15 mm.

In the measured spectral characteristics presented in Fig. 1, characteristic minima related to the coupling of the input light to individual modes of the structure can be observed. By the time of writing this article, no work presenting a method for determining all the modes of TFBG structures had been published; therefore, this article presents a short analysis that allows the proposal of such a method. Although there are works in which the authors present changes in the power of individual modes or groups of modes [23, 24], there is no study in which all the modes are numbered and counted. Such numbering is possible for each TFBG structure, and

Metrol. Meas. Syst., Vol. 30 (2023), No. 3, pp. 507–518
DOI: 10.24425/mms.2023.146418

its representation is definitely facilitated by dividing the entire spectrum into 4 characteristic spectral regions, as shown in Fig. 1. The first region from the right, the Bragg mode area, is associated with the so-called Bragg reflection and corresponds to the Bragg mode with azimuthal number $m = 0$. The only excited mode has a radial number equal to 1. Therefore, this mode is labeled LP_{01}. The ghost mode area in Fig. 1 includes the so-called ghost mode. This mode is the result of accumulated cladding modes. The spectral overlap of these modes results from similar wavelengths corresponding to these modes. In many papers, the ghost mode in a TFBG is labeled by the sum of low-order modes with azimuthal number equal to 1. However, this is not a precise label and results in ambiguities in the numbering of the modes, which is why publications simply give the azimuthal and radial number mode without indicating the spectral characteristics, *e.g.*, [21]. The abovementioned simplification of labeling the ghost mode as LP_{1n} results from the fact that this region (second region from the right in Fig. 1) consists of several modes with azimuthal number $m = 0$. Only in Tuan Guo *et al.*, published in 2016 in the journal *Optics & Laser Technology* [20], were numerical calculations of individual modes of propagating light carried out. Calculations were made separately for each mode, and the entire spectral characteristics of a TFBG (4°), which they obtained, resulted from the combination of all component modes. [20] is crucial in understanding the appropriate numbering of modes in TFBG structures, although the authors, despite having such important results, did not present a full characterization of all the modes of the TFBG structure. Only by combining the knowledge from this publication with consideration of the method of numbering higher-order modes (alternately with azimuthal number 0 or 1) in work [21] – Figs. 15, 17, and 19 – or, *e.g.*, article [22] – Fig. 4 – and conclusions from observations of TFBG structure characteristics under different light input conditions can all the linearly polarized modes be fully determined based on the transmission spectral characteristics.

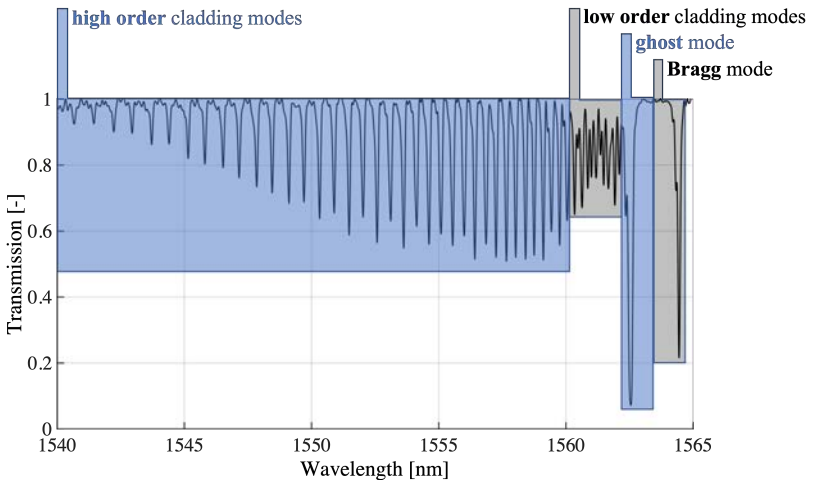

Fig. 1. Spectral characteristics of the TFBG with four modal regions highlighted.

2. Modeling of light intensity distribution of propagating modes in TFBG structures

The appearance of a disturbance in the form of a tilted Bragg grating in a single-mode fiber results in the coupling of light introduced into the optical fiber propagating in the core to a series of cladding modes. These modes have a strictly defined power distribution, which means that

the intensity of light propagating in individual modes is strictly defined. These intensities can be determined by numerically solving the eigenvalue equation for the LP modes [25]. The easiest way to begin this task is to start with Maxwell's equation, which can be written as a wave equation in the form:

$$\begin{aligned} \nabla^2 \overline{E}_z + n^2(\omega) k_0^2 \overline{E}_z = 0 \\ \nabla^2 \overline{H}_z + n^2(\omega) k_0^2 \overline{H}_z = 0 \end{aligned}, \tag{1}$$

where ∇^2 is the Laplace operator, ω is the angular frequency, k_0 is the wavenumber, with $k_0 = \omega/c$, and the refractive index n is written as a function of the angular frequency $n(\omega)$. Note that $n = n_1$ inside the core, but it takes a value equal to n_2 in the cladding. After writing the independent components E_z and H_z in cylindrical coordinates ρ, φ, and z and separating the variables, the general solution for E_z and H_z is:

$$E_z = \begin{cases} C_1 J_m(p\varrho) e^{im\varphi} e^{i\beta z}; & \varrho \le a, \\ C_2 K_m(q\varrho) e^{im\varphi} e^{i\beta z}; & \varrho > a, \end{cases} \qquad H_z = \begin{cases} C_3 J_m(p\varrho) e^{im\varphi} e^{i\beta z}; & \varrho \le a, \\ C_4 K_m(q\varrho) e^{im\varphi} e^{i\beta z}; & \varrho > a, \end{cases} \tag{2}$$

wherein:

$$p^2 = n_1^2 k_0^2 - \beta^2, \tag{3}$$

and:

$$q^2 = \beta^2 - n_2^2 k_0^2 . \tag{4}$$

C_1, C_2, C_3, and C_4 are constants determined by the boundary conditions, and β is the phase constant or so-called propagation constant. The function J_m is a Bessel function of the first kind and m order, while the function K_m is a Bessel function of the second kind and m order, and a is the core radius. After writing down the remaining quantities as functions of E_z and H_z and considering the boundary conditions that assume continuity of the magnetic field and the electric field at the core-cladding boundary, the eigenvalue equation can be formulated in the form:

$$\left(\frac{J'_m(pa)}{pJ_m(pa)} + \frac{K'_m(qa)}{qK_m(qa)} \right) \cdot \left(\frac{J'_m(pa)}{pJ(pa)} + \frac{n_2^2}{n_1^2} \frac{K'_m(qa)}{qK_m(qa)} \right) = \frac{m^2}{a^2} \left(\frac{1}{p^2} + \frac{1}{q^2} \right) \cdot \left(\frac{1}{p^2} + \frac{n_2^2}{n_1^2} \frac{1}{q^2} \right). \tag{5}$$

The eigenvalue equation contains Bessel functions and their derivatives, which allows its numerical solution.

We also introduce a dimensionless parameter V in terms of the normalized frequency, which is equal to:

$$V = k_0 a \sqrt{n_1^2 - n_2^2} . \tag{6}$$

Therefore, there are many solutions β for a given value of V. Each of these solutions represents an optical mode. The number of modes strongly depends on the value of V. The effective mode refractive index can be defined as:

$$n_{\text{eff}} = \frac{\beta}{k_0} . \tag{7}$$

Its value is between n_1 and n_2 for all cladding modes. At this point, it is useful to introduce a normalized quantity b in the form:

$$b = \frac{n_{\text{eff}} - n_2}{n_1 - n_2} , \tag{8}$$

Metrol. Meas. Syst., Vol. 30 (2023), No. 3, pp. 507–518
DOI: 10.24425/mms.2023.146418

with $0 < b < 1$. There are many solutions to (5) for each quantity m. The modes are designated HE_{mn} or EH_{mn} ($n = 1, 2, \ldots$) depending on whether H_z or E_z is dominant. TE and TM modes exist for $m = 0$ and are called TE_{0n} and TM_{0n} modes. Assuming $m = 0$ in eigenvalue equation (5), two equations are obtained:

$$\left(\frac{J'_m(pa)}{pJ_m(pa)} + \frac{K'_m(qa)}{qK_m(qa)}\right) = 0, \qquad \left(\frac{J'_m(pa)}{pJ_m(pa)} + \frac{n_2^2}{n_1^2}\frac{K'_m(qa)}{qK_m(qa)}\right) = 0. \tag{9}$$

These equations therefore describe the fiber modes TE_{0n} and TM_{0n}. For weakly conducting fibers, where $n_1 - n_2 \ll 1$, the eigenvalue equation can be significantly simplified to the following form:

$$\left(\frac{J'_m(pa)}{pJ_m(pa)} + \frac{K'_m(qa)}{qK_m(qa)}\right)^2 = \frac{m^2}{a^2}\left(\frac{1}{p^2} + \frac{1}{q^2}\right)^2. \tag{10}$$

Using the properties of the Bessel function, eigenvalue equation (5) can be written in a simplified form:

$$p\frac{J_{l-1}(pa)}{J_l(pa)} = -q\frac{K_{l-1}(qa)}{K_l(qa)}, \tag{11}$$

with $l = 1$ for TE and TM modes, $l = m - 1$ for HE modes and $l = m + 1$ for EH modes. The modes $TE_{0,n}$ and $TM_{0,n}$ are so-called degenerate modes. Additionally, modes $HE_{m+1,n}$ and $EH_{m+1,n}$ are degenerate modes. Degenerate modes travel at the same speed through the fiber. Any linear combination of degenerate modes will propagate through the fiber without changing shape. Some linearly polarized combinations give rise to LP_{mn} modes. For example, LP_{0n} modes are composed of HE_{1n} modes, LP_{1n} modes are composed of TE_{0n}+ TM_{0n}+ HE_{2n} modes, and LP_{mn} modes are composed of $HE_{m+1,n}$+ $EH_{m-1,n}$ modes.

Equation (11) can be numerically solved. The results of light intensity calculations corresponding to selected LP modes are presented in the subsequent part of this article. All results were obtained for the core diameter $a = 8$ µm and for the core and cladding refractive indices $n_1 = 1.4624$ and $n_2 = 1.4574$, respectively.

3. Identification of individual LP modes based on TFBG spectral characteristics

Returning to the analysis of the Bragg mode area in Fig. 1, we are dealing with one clear minimum here. This is the LP_{01} mode which propagates mainly in the core of the optical fiber. In the second spectral region in Fig. 1, *i.e.*, the ghost mode area, we are also dealing with one clear minimum corresponding to the modes that make up the ghost peak. The shapes of the minima coming from the Bragg mode and the ghost mode are shown in Fig. 2.

The spectral characteristics presented in Fig. 2 in the spectral ranges corresponding to the Bragg mode and the ghost mode were measured for the TFBG structure with a tilt angle of 2° and a length of 15 mm. Analyzing the results presented in [20], the largest contribution to the power transmission in this wavelength region is made by the LP_{11}, LP_{12}, LP_{13}, and LP_{14} modes with azimuthal number $m = 1$. There are also modes with azimuthal numbers $m = 2$ (LP_{21}, LP_{22}, LP_{23}, LP_{24}) and $m = 3$ (LP_{31}, LP_{32}, LP_{33}, LP_{34}); however, their contributions to the transmission of the light wave in the waveguide are negligible. The existence of modes with azimuthal number $m = 0$ corresponding to the Bragg mode but with higher radial numbers $n = 2 - 4$ is also characteristic. These are the LP_{02}, LP_{03}, and LP_{04} modes and they are also part of the entire ghost mode peak, making up its left part, being the most advanced ghost modes on the shorter wavelength side.

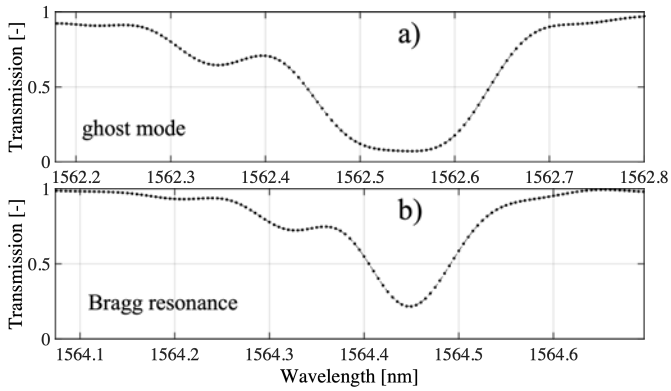

Fig. 2. Spectral characteristics in the spectral ranges corresponding to the a) Bragg mode and b) ghost mode.

The information above enables determination of the modes of the measured TFBG characteristics in the Bragg and ghost mode areas, *i.e.*, those constituting the spectral ranges corresponding to the Bragg mode and ghost mode minima. Figure 3 shows the spectral characteristics of the TFBG structure in the analyzed spectral range, measured at a temperature of 20°C, in the free state and the bent state, with the input light polarization consistent with the P state [11].

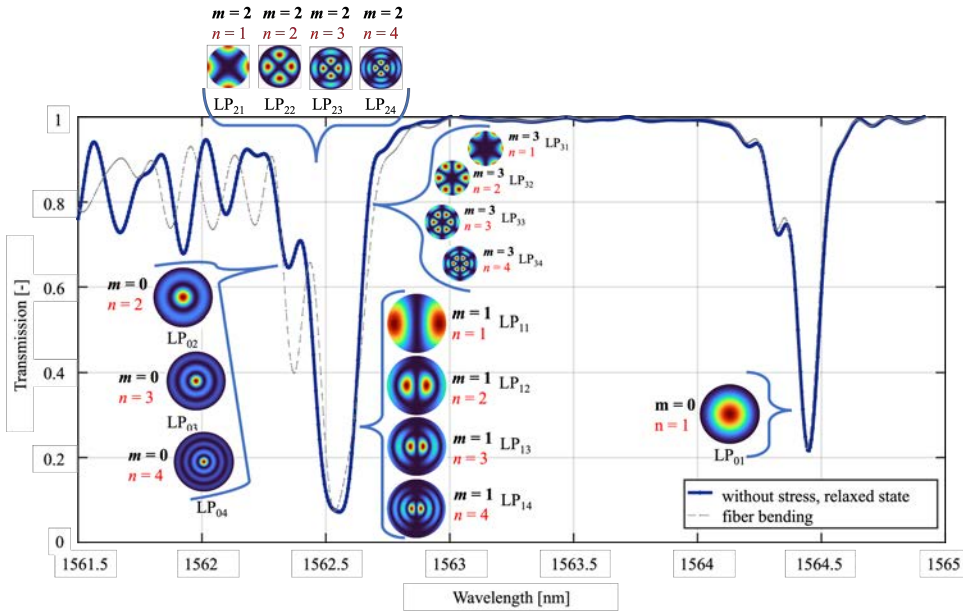

Fig. 3. Designation of modes with azimuthal numbers $m = 0{-}3$ based on actual characteristics of the TFBG in the regions of the Bragg mode and the ghost mode.

The two spectral regions not yet discussed include the high-order cladding mode and low-order cladding mode areas. Figure 4 presents the measured spectral characteristics showing the minima coming from low-order cladding modes.

Metrol. Meas. Syst., Vol. 30 (2023), No. 3, pp. 507–518
DOI: 10.24425/mms.2023.146418

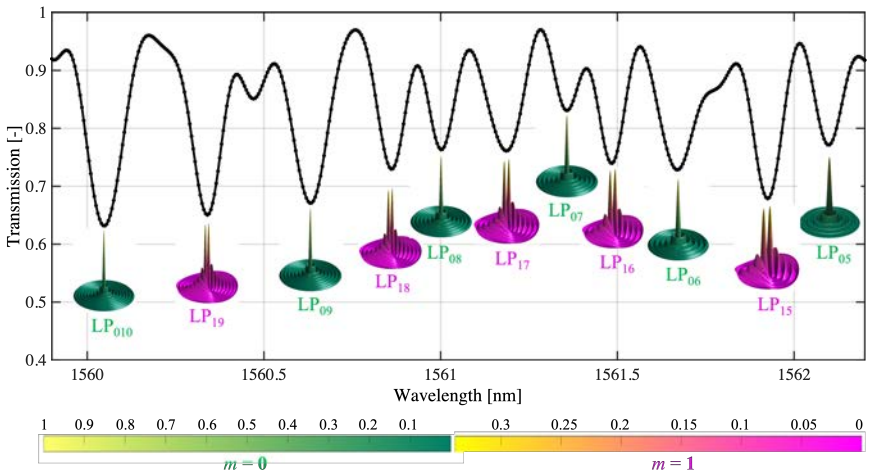

Fig. 4. Designation of TFBG cladding modes in the low-order cladding mode area.

As can be seen, the minima coming from individual modes have irregular amplitudes, which does not prevent them from being labeled and counted. The low-order cladding mode area, on the one hand, is characterized by the largest differences in the amplitudes and widths of peaks originating from low-order cladding modes. At the same time, the sensitivity of shape changes and shifts of these peaks to changes in light propagation conditions (caused, for example, by bending) in the entire structure is the largest [13].

The high-order cladding mode area has regular minima amplitudes in the transmission characteristics coming from individual cladding modes. In the case of a TFBG recorded in a single-mode fiber, modes with azimuthal numbers of 0 and 1 are excited, and they alternate for successive wavelengths [21]. The designation of these modes based on the spectral characteristics is shown in Fig. 5. Figures 5–6 show the measured transmission characteristics of the TFBG in the high-order cladding mode area.

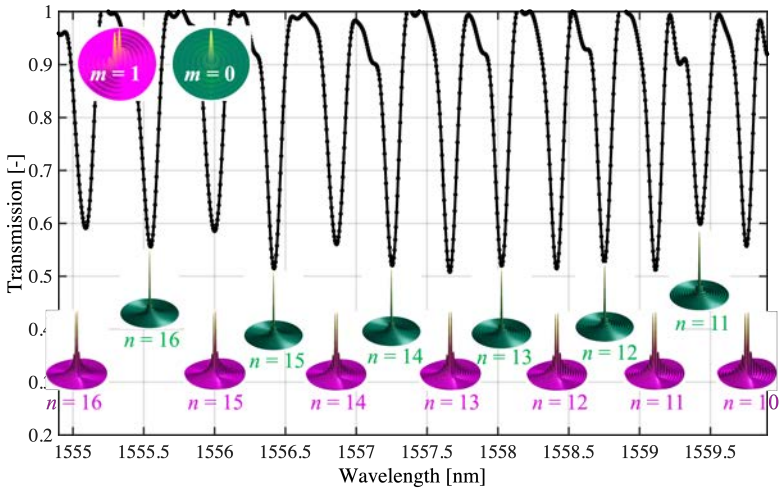

Fig. 5. Designation of the TFBG cladding modes in the high-order cladding mode area for $m = 0–1$ and $n = 10–16$.

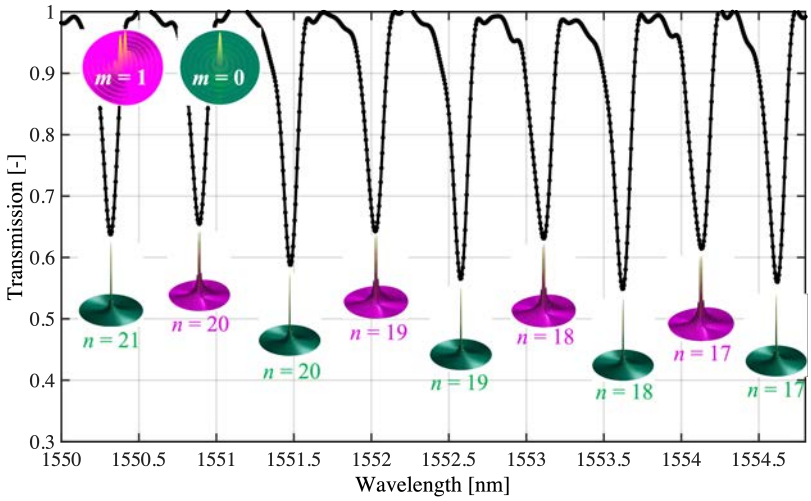

Fig. 6. Designation of the TFBG cladding modes in the high-order cladding mode area for $m = 0-1$ and $n = 17-21$.

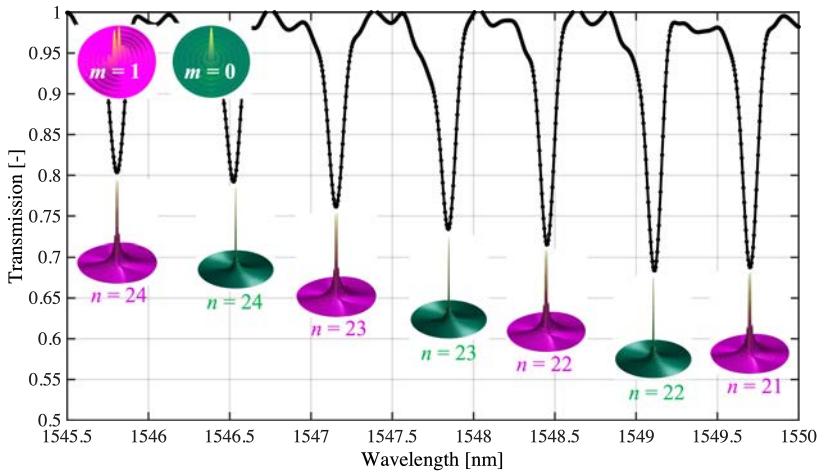

Fig. 7. Designation of the TFBG cladding modes in the high-order cladding mode area for $m = 0-1$ and $n = 21-24$.

The individual azimuthal and radial numbers of cladding modes are labeled in the figures. For the TFBG structure with a tilt angle equal to 2°, a length of 15 mm and the Bragg mode for the wavelength of 1564.4 nm, the high-order cladding mode area is in the spectral range of 1540.5 nm–1560 nm. The spectral range from 1560 nm to 1562.25 nm belongs to the low-order cladding mode area (Fig. 1) and is 10 times narrower than that corresponding to the high-order cladding mode area. The modes in the spectral range corresponding to the high-order cladding mode area are most often used as markers of changes in the factors acting on the TFBG [26]. Figure 8 shows the highest-order modes with radial numbers up to 27 and 28 and azimuthal numbers of 1 and 0, respectively. The LP_{028} mode is the last visible mode in the transmission characteristics of the TFBG with a tilt angle of 2°.

Metrol. Meas. Syst., Vol. 30 (2023), No. 3, pp. 507–518
DOI: 10.24425/mms.2023.146418

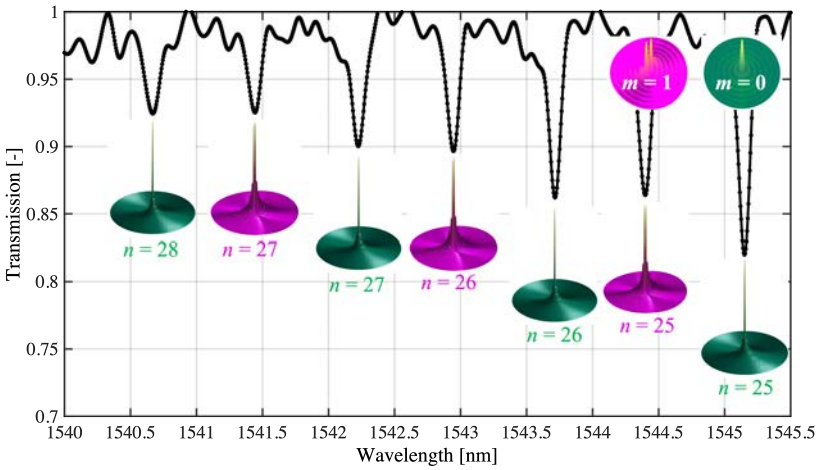

Fig. 8. Designation of the TFBG cladding modes in the high-order cladding mode area for $m = 0-1$ and $n = 25-28$.

4. Conclusions

This paper presents a method for labeling all the significant propagating modes in TFBG structures. Correct mode designation is important when using TFBGs in specific measurement systems. The use of these structures to determine changes in quantities affecting their spectral characteristics requires the measurement of the transmission losses, half-width or shift of a given TFBG mode. This, in turn, requires the selection of the appropriate spectral range and the selection of changes, most often of one specific mode. It is therefore important to properly determine the modes of such structures. This also has a key impact on the possibility of explaining the phenomena causing changes in transmission for specific wavelengths because knowledge of the azimuthal and radial numbers of modes allows determination of spatial distribution of light intensity in the TFBG optical waveguide. This, in turn, makes it possible to explain the phenomenon of changes in radiation intensity due to disturbances caused in the waveguide, *e.g.*, bending and stretching.

Acknowledgements

This work is supported by grant from the Ministry of Science and higher Education of the Republic of Kazakhstan within the framework of the Project No. AP09259547 “Development of a system of distributed fiber-optic sensors based on fiber Bragg gratings for monitoring the state of building structures”, carried out by the Institute of Information and Computational Technologies CS MSHE RK.

References

[1] Skorupski, K., & Mroczka, J. (2014). Effect of the necking phenomenon on the optical properties of soot particles. *Journal of Quantitative Spectroscopy and Radiative Transfer*, *141*, 40–48. https://doi.org/10.1016/j.jqsrt.2014.03.001

[2] Mroczka, J., & Szczuczyński, D. (2013). Improved technique of retrieving particle size distribution from angular scattering measurements. *Journal of Quantitative Spectroscopy and Radiative Transfer*, *129*, 48–59. https://doi.org/10.1016/j.jqsrt.2013.05.030

[3] Świrniak, G., & Mroczka, J. (2022). Forward and inverse analysis for particle size distribution measurements of disperse samples: A review. *Measurement*, *187*, 110256. https://doi.org/10.1016/j.measurement.2021.110256

[4] Frieden, J., Cugnoni, J., Botsis J., Gmür, T., & Ćorić, D. (2010). High-speed internal strain measurements in composite structures under dynamic load using embedded FBG sensors. *Composite Structures*, *92*(8), 1905–1912. https://doi.org/10.1016/j.compstruct.2010.01.007

[5] Skorupski, K., Harasim, D., Panas, P., Cięszczyk, S., Kisała, P., Kacejko, P., Mroczka, J., & Wydra, M. (2020). Overhead Transmission Line Sag Estimation Using the Simple Opto-Mechanical System with Fiber Bragg Gratings – Part 2: Interrogation System. *Sensors*, *20*(9), 2652. https://doi.org/10.3390/s20092652

[6] Liu, M.-Y. Zhou, S.-G. Song, H. Zhou, W.-J., & Zhang, X. (2018). A novel fibre Bragg grating curvature sensor for structure deformation monitoring. *Metrology and Measurement Systems*, *25*(3), 577–587. https://doi.org/10.24425/123899

[7] Detka, M., & Kaczmarek, Z. (2013). Distributed Strain Reconstruction Based on a Fiber Bragg Grating Reflection Spectrum. *Metrology and Measurement Systems*, *1*, 53–64. https://doi.org/10.2478/mms-2013-0005

[8] Imas, J. J., Albert, J., Del Villar, I., Ozcáriz, A., Zamarreño, C. R., & Matías, I. R. (2022). Mode Transitions and Thickness Measurements During Deposition of Nanoscale TiO2 Coatings on Tilted Fiber Bragg Gratings. *Journal of Lightwave Technology*, *40*(17), 6006–6012. https://doi.org/10.1109/JLT.2022.3186596

[9] Ooi, Ch.-W., Low, M. L., Udos, W., Lim, K.-S. & Ahmad, H. (2022). Novel Schiff base functionalized 80-μm tilted fiber Bragg grating chemosensor for copper(II) ion detection. *Optical Fiber Technology*, *71*, 102920. https://doi.org/10.1016/j.yofte.2022.102920

[10] Cięszczyk, S., Harasim, D., & Kisała, P. (2018). Novel twist measurement method based on TFBG and fully optical ratiometric interrogation. *Sensors and Actuators A*, *272*, 18–22. https://doi.org/10.1016/j.sna.2018.01.048

[11] Harasim, D., Kisała P., Yeraliyeva, B., & Mroczka J. (2021). Design and Manufacturing Optoelectronic Sensors for the Measurement of Refractive Index Changes under Unknown Polarization State. *Sensors*, *21*(21), 7318. https://doi.org/10.3390/s21217318

[12] Harasim, D., & Cięszczyk, S. (2022). A novel method of elimination of light polarization cross sensitivity on tilted fiber Bragg grating bending sensor. *Metrology and Measurement Systems*, *29*(4), 737–749. https://doi.org/10.24425/mms.2022.143066

[13] Kisała, P. (2022). Physical foundations determining spectral characteristics measured in Bragg gratings subjected to bending. *Metrology and Measurement Systems*, *29*(3), 573–584. https://doi.org/10.24425/mms.2022.142275

[14] Takeda, S., Sato, M., & Ogasawara T. (2022). Simultaneous measurement of strain and temperature using a tilted fiber Bragg grating. *Sensors and Actuators A: Physical, 335*, 113346. https://doi.org/10.1016/j.sna.2021.113346

[15] Zhu, F., Hao, X., Zhang, Y., Jia, P., Su, J., Wang, L., Liu, L., Xi, L., & An, G. (2022). D-shaped optic fiber temperature and refractive index sensor assisted by tilted fiber Bragg grating and PDMS film. *Sensors and Actuators A: Physical*, *346*, 113870. https://doi.org/10.1016/j.sna.2022.113870

[16] Tolegenova, A., Kisała, P., Zhetpisbayeva, A., Mamyrbayev, O., & Medetov, B. (2019). Experimental determination of the characteristics of a transmission spectrum of tilted fiber Bragg gratings. *Metrology and Measurement Systems*, *26*(3), 581–589. https://doi.org/10.24425/mms.2019.129585

Metrol. Meas. Syst., Vol. 30 (2023), No. 3, pp. 507–518
DOI: 10.24425/mms.2023.146418

[17] Harasim, D. (2017). The Influence of Fibre Bending on Polarization-Dependent Twist Sensor Based on Tilted Bragg Grating. *Metrology and Measurement Systems*, *24*(3), 577–584. https://doi.org/10.1515/mms-2017-0038

[18] Kisała, P., Skorupski, K., Cięszczyk, S., Panas, P., & Klimek J. (2018). Rotation and twist measurement using tilted fibre Bragg gratings. *Metrology and Measurement Systems*, *25*(3), 429-440. https://doi.org/10.24425/123893

[19] Van, L. C., Le Tran, B. T., Van, T. D., Minh, N. V. T., Thi, T. N., Thi, H. P. N., & Nguyen, M. H. T. (2023). Supercontinuum generation in highly birefringent fiber infiltrated with carbon disulfide. *Optical Fiber Technology*, *75*, 103151. https://doi.org/10.1016/j.yofte.2022.103151

[20] Guo, T., Liu, F., Guan, B.-O., & Albert, J. (2016) [INVITED] Tilted fiber grating mechanical and biochemical sensors. *Optics & Laser Technology*, *78, Part B*, 19–33. https://doi.org/10.1016/j.optlastec.2015.10.007

[21] Dong, X., Zhang, H., Liu, B., & Miao, Y. (2011). Tilted fiber Bragg gratings: Principle and sensing applications. *Photonic Sensors*, *1*, 6–30. https://doi.org/10.1007/s13320-010-0016-x

[22] Laffont, G., & Ferdinand, P. (2001). Tilted short-period fibre-Bragg-grating- induced coupling to cladding modes for accurate refractometry. *Measurement Science and Technology*, *12*(7), 765–770. https://doi.org/10.1088/0957-0233/12/7/302

[23] Feng, W., & Niu, S. (2023). Intensity-modulated liquid-level and temperature sensor based on cascaded air bubble and fiber Bragg grating interferometer. *Sensors and Actuators A: Physical*, 354, 114300. https://doi.org/10.1016/j.sna.2023.114300

[24] Yang K., Liu Y.-G., Wang Z., Li G.-Y., Han Y., Zhang H.-W., & Yu J. (2018). Five-wavelength-switchable all-fiber erbium-doped laser based on few-mode tilted fiber Bragg grating. *Optics & Laser Technology*, 108, 273–278. https://doi.org/10.1016/j.optlastec.2018.07.005

[25] Pollock, C. R., & Lipson, M. (2003). *Photonic Crystals. In: Integrated Photonics*. Springer, Boston, MA. https://doi.org/10.1007/978-1-4757-5522-0_13

[26] Lobry, M., Loyez, M., Debliquy, M., Chah, K., Goormaghtigh, E. & Caucheteur, Ch. (2023). Electroplasmonic-assisted biosensing of proteins and cells at the surface of optical fiber. *Biosensors and Bioelectronics*, 220, 114867. https://doi.org/10.1016/j.bios.2022.114867

Piotr Kisała received a diploma in informatics and computer networks from Maria Curie-Skłodowska University, Poland. He received the Ph.D. degree in 2009 and Habilitation degree in 2013 and the title of professor in 2020. He is currently head of Optoelectronic & ICT Department at LUT. His research interests include optical sensor projects, fabrication and testing and the design and development of unconventional FBG sensors. Prof. Kisała has authored over 80 journal publications and conference contributions and 6 patents.

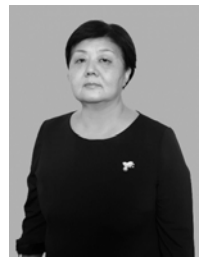

Aliya Kalizhanova graduated from the Faculty of Mechanics and Mathematics of Novosibirsk State University. In 2003, she received the degree of Candidate of Physical and Mathematical Sciences and the title of professor in 2018. She is head of the scientific project of grant financing of the Information and Computational Technologies CS MSHE RK AR05132778, AP09259547. Her scientific interests include mathematical modeling of systems, models of transport systems network analysis, optimization methods, technologies for developing sensor systems for signals receive-transmit, mathematical modeling of Bragg fiber gratings. She is the author of more than 150 journal publications and conference materials, as well as 8 patents.

Ainur Kozbakova received a diploma in the specialty "Software of computer technology and automated systems" at the K.I. Satpayev Kazakh National Technical University, in 2017 she received a PhD in 6D070300 – Information Systems and the title of Associate Professor in 2020. Her research interests are development of mathematical models and methods of designing information systems and applied software, automation of information processes. She is the author of more than 70 journal publications and conference materials, as well as 7 patents.

Bakhyt Yeraliyeva received her diploma in the field of automation and computer networks from M.Kh. Dulaty Taraz State University, Kazakhstan. She received her Master of Engineering degree in 2014. Since 2018, she has been a doctoral student at the Lublin University of Technology, at the Faculty of Electrical Engineering and Informatics. Currently she works as a senior lecturer at the Department of Information Systems at the M.Kh. Dulaty Taraz State University. Her research interests include information systems, fiber optic technologies, microprocessor systems. She is the author of more than 40 publications and conference papers.